Numerical simulation of metal-halide lamp using a time-dependent two-dimensional model

S. Hashiguchi
Department of Electronics and Information Science, Kyoto Institute of Technology, Matugasaki, Sakyo-ku, Kyoto 606-8585, Japan

K. Hatase and S. Mori
Lighting Equipment Division, Japan Storage Battery, Co., Ltd., Nishinosho, Kisshoin, Minami-ku, Kyoto 601-8520, Japan

K. Tachibana[a)]
Department of Electronics Science and Engineering, Kyoto University, Yoshida Honmachi, Sakyo-ku, Kyoto 606-8317, Japan

(Received 12 February 2002; accepted for publication 23 April 2002)

Numerical simulation of a vertically held metal-halide lamp (Hg/Na/Sc system) is presented. The lamp was driven by an ac current of 60 Hz. The model took convection and diffusion of various species into account. A method for rapid calculation of optically thick radiation power was developed. Density of scandium ions and sodium ions has a minimum on the central axis due to radial ambipolar diffusion. Density of metallic atoms and ions and metal iodine molecules decreases with increasing axial distance from the bottom of the tube. This tendency was explained by convection and diffusion. The density of scandium ions depends on the direction of the current; the density was greater at upward current than at downward current. © *2002 American Institute of Physics.* [DOI: 10.1063/1.1486255]

I. INTRODUCTION

High-pressure mercury lamps with metal-halide additives are widely used. The principal role of additives is to give the light source better energy efficiency and a more satisfactory color than there would be otherwise. A computer-aided study may be useful to determine the effects of each of the various additives on the discharge.

The main purpose of this simulation is to determine temperature and the number densities of various kinds of particles including ions and electrons, and how they contribute to the lamp's optical and electrical properties. Hashiguchi, Mori, and Tachibana[1] modeled high-pressure mercury discharge lamps; the energy equation coupled with momentum and continuity equations was solved to obtain temperature and convection velocity. The contribution of optically thick lines to radiation power was the subject of exact analysis. We have to consider all these problems in order to model metal-halide lamps. In addition, we have to develop a method to determine the number densities of various kinds of particles which result from metal-halide additives; the diffusion of these particles as well as convection have to be taken into account. Dakin, Rautenberg, and Goldfield[2] modeled a Hg/Na/Sc system taking all these properties into account. Their model was complicated and it was not well suited for practical purposes, although they gave temperature and number densities of several kinds of particles for dc operation. Ishigami[3] made a more practical model but neglected convection and diffusion. He solved the energy equation together with the equilibrium relations between species to obtain temperature and the number densities of various kinds of particles as a function of radial distance. He obtained the optical and electrical properties of the lamp for time-dependent as well as time-independent operation.

We present a time-dependent model which is applied to various kinds of particles taking convection and diffusion into account. A method for the rapid calculation of optically thick radiation power has been developed and we are able to calculate for several tens of periods in a reasonable computing time with this model. We will make a comparison with this experiment in a later article.

Section II describes a fluid model. Sections III through V describe transport coefficients, radiation power, and numerical method, respectively. Section VI describes results and a discussion of the model, and Sec. VII contains concluding remarks.

II. MODELING A METAL-HALIDE LAMP

We simulate discharge in a vertically held metal-halide lamp which is shown in Fig. 1; the tube is a circular cylinder and both upper and lower boundaries are replaced by circular planes which are given as dotted lines to simplify calculation. We assume that local thermal equilibrium holds throughout the region of calculation. The lamp is driven by an ac current of 60 Hz. The dissipation time of thermal energy due to radiation is the same order of magnitude as the period of driving current and we demonstrate the time-dependent energy equation. The radial temperature gradient induces convection due to buoyancy and we must solve the equation of motion simultaneously with the energy equation. The partial pressures of additives are small compared with

a)Electronic mail: tatibana@kuee.kyoto-u.ac.jp

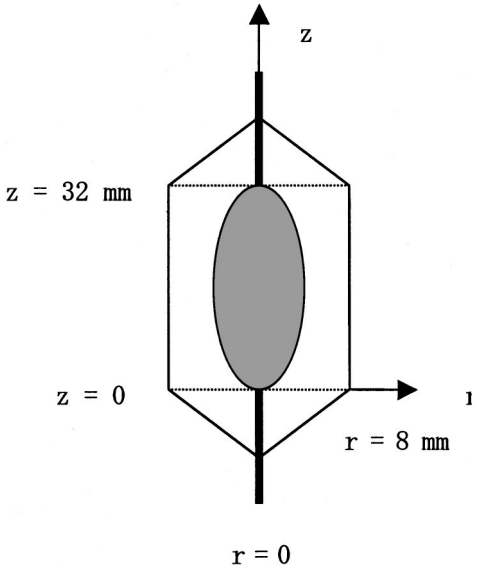

FIG. 1. Schematic drawing of cylindrical vessel of a metal-halide lamp with axial and radial dimensions. Calculating region is the area bounded by side lines corresponding to sidewalls and upper and lower dotted lines corresponding to upper and lower bases.

the pressure of mercury and we use a one-fluid model to determine the gas temperature and the convection velocity, although radiation power and transport coefficients also depend on the partial pressures of additives. Change in pressure propagates in the gas with sound velocity and the characteristic time of change in pressure in the tube is much smaller than the period of driving current. Hence, we can safely use steady state solutions for momentum equations and the continuity equation. The vertically standing tube has a symmetry around the central axis and all physical quantities depend on the radial position r and the axial position z but they do not depend on the azimuthal angle. Equations (1) through (3) give the continuity equation and momentum equations[1]

$$\frac{1}{r}\frac{\partial}{\partial r}(r\rho u)+\frac{\partial}{\partial z}(\rho v)=0, \tag{1}$$

$$\frac{1}{r}\frac{\partial}{\partial r}(r\rho u^2)+\frac{\partial}{\partial z}(\rho uv)-\frac{1}{r}\frac{\partial}{\partial r}\left(r\nu\frac{\partial u}{\partial r}\right)-\frac{\partial}{\partial z}\left(\nu\frac{\partial u}{\partial z}\right) =-\frac{\partial p}{\partial r}-\nu\frac{u}{r^2} \tag{2}$$

and

$$\frac{1}{r}\frac{\partial}{\partial r}(r\rho uv)+\frac{\partial}{\partial z}(\rho v^2)-\frac{1}{r}\frac{\partial}{\partial r}\left(r\nu\frac{\partial v}{\partial r}\right)-\frac{\partial}{\partial z}\left(\nu\frac{\partial v}{\partial z}\right) =-\frac{\partial p}{\partial z}-\rho g, \tag{3}$$

where ρ is mass density, u and v are radial and axial velocities, respectively, ν is viscosity, p is pressure, and g is acceleration due to gravity. Equation (4) gives the time-dependent energy balance[1]

$$\frac{\partial q}{\partial t}+\frac{1}{r}\frac{\partial(rhu)}{\partial r}+\frac{\partial(hv)}{\partial z}-\frac{1}{r}\frac{\partial}{\partial r}\left(rk\frac{\partial T}{\partial r}\right)-\frac{\partial}{\partial z}\left(k\frac{\partial T}{\partial z}\right) =\sigma E^2-U, \tag{4}$$

where q and h are, respectively, internal energy and enthalpy in unit volume, k is thermal conductivity, σ is electrical conductivity, E is axial electric field, and $-U$ is radiative power loss in unit volume. We neglect the kinetic energy of fluid and the work done by shearing stress due to viscosity because flow energy is much less than thermal energy. We also neglect the difference in the potential energy of gravity in the tube compared with thermal energy.

Thermal conductivity and electrical conductivity depend on the number densities of ions and electrons. Radiation power U includes line radiation from sodium atoms, scandium atoms and scandium ions as well as that from mercury atoms. Therefore, we have to determine the number densities of these species to obtain k, σ and U in Eq. (4). Condensates of metal iodides are introduced in the tube because metal iodides have considerable values of vapor pressure at temperatures around 1000 K. We consider the number densities of the following nine species as unknown variables: Hg^+, Na, Na^+, Sc, Sc^+, e(electron), I(iodine), NaI and ScI_3. We take the pressure of mercury gas as the total pressure because the partial pressures of additives are much smaller and the dynamic pressure resulting from velocity is much less than the static pressure. Hence, we determine the number density of mercury atoms as a function of temperature because the total pressure is uniform in the closed discharge tube.

It may be possible to determine the number density of each species by solving the continuity equation for each species which is expressed as

$$\frac{\partial n_k}{\partial t}+\nabla\cdot\boldsymbol{\phi}_k=S_k, \tag{5}$$

where n is number density, ϕ is particle flux vector, and S is net creation rate of the species. Here, subscript k denotes kind of species. Because we assume thermal equilibrium, we can use equilibrium relations for ionization and dissociation, which are independent of the creation and annihilation processes included in S

$$\frac{n_{Na^+}n_e}{n_{Na}}=K_1,\quad \frac{n_{Sc^+}n_e}{n_{Sc}}=K_2,\quad \frac{n_{Hg^+}n_e}{n_{Hg}}=K_3,\quad \frac{n_{Na}n_I}{n_{NaI}}=K_4,\quad \frac{n_{Sc}n_I^3}{n_{ScI_3}}=K_5, \tag{6}$$

where K_1 through K_5 are equilibrium constants which depend on temperature. Another relation which we can use is the charge neutrality condition

$$n_{Na^+}+n_{Sc^+}+n_{Hg^+}=n_e. \tag{7}$$

This equation holds in the discharge tube except in the thin sheath region near the boundary. We apply Eq. (7) throughout the region of calculation shown in Fig. 1. We have to determine number densities of nine species but we have only six independent equations given in Eqs. (6) and (7). The condition that each element is neither created nor annihilated during the discharge gives the conservation equations for sodium, scandium, and iodine elements. This condition holds in any point in the discharge tube and is expressed by the following relations using the net creation rate S for Na, Sc and I

$$S_{Na}+S_{Na^+}+S_{NaI}=0, \quad S_{Sc}+S_{Sc^+}+S_{ScI_3}=0,$$

$$S_I+S_{NaI}+3S_{ScI_3}=0.$$

The above relations are expressed by number densities by using Eq. (5).

$$\frac{\partial}{\partial t}(n_{Na}+n_{Na^+}+n_{NaI})+\nabla(\phi_{Na}+\phi_{Na^+}+\phi_{NaI})=0, \tag{8}$$

$$\frac{\partial}{\partial t}(n_{Sc}+n_{Sc^+}+n_{ScI_3})+\nabla(\phi_{Sc}+\phi_{Sc^+}+\phi_{ScI_3})=0, \tag{9}$$

$$\frac{\partial}{\partial t}(n_I+n_{NaI}+3n_{ScI_3})+\nabla(\phi_I+\phi_{NaI}+3\phi_{ScI_3})=0. \tag{10}$$

Hence, we obtain nine equations for nine unknown number densities. The particle flux density vector includes convection and diffusion for neutral particles and is expressed as

$$\phi_n=n_n\mathbf{w}-D_n\left(\nabla n_n+\frac{n_n}{T}\nabla T\right), \tag{11}$$

where w is the convection velocity whose radial and axial components are u and v, respectively, and subscript n means neutral particle. The diffusion term includes the effect of temperature gradient. The particle flux for ions is more complex; the radial component ψ_{ion} includes ambipolar diffusion and axial component ξ_{ion} includes drift due to axial electric field

$$\psi_{ion}=n_{ion}u-D_{ion}\left(\frac{\partial n_{ion}}{\partial r}+\frac{n_{ion}}{n_e}\frac{\partial n_e}{\partial r}+2\frac{n_{ion}}{T}\frac{\partial T}{\partial r}\right). \tag{12}$$

$$\xi_{ion}=n_{ion}(v+v_{d,ion})-D_{ion}\left(\frac{\partial n_{ion}}{\partial z}+\frac{n_{ion}}{T}\frac{\partial T}{\partial z}\right),$$

$$v_{d,ion}=\mu_{ion}E. \tag{13}$$

Here, ψ_{ion} includes ambipolar diffusion due to multiple kinds of ions with temperature gradient and ξ_{ion} includes drift velocity due to axial electric field; the mobility μ_{ion} is determined from D_{ion} using Einstein's relation. Equations (11) and (12) are derived in the Appendix.

III. TRANSPORT COEFFICIENTS

Collisions between particles determine transport coefficients which are the averaged quantities over many particles; we make an averaging procedure using Maxwellian velocity distribution. The working gas consists of several kinds of particles and we estimate the contribution of each particle to each of the transport coefficients.

A. Viscosity

Heavier particles contribute more to viscosity. The mercury atom is one of the heavy particles and it is the dominant component. Therefore, the viscosity is totally determined by collisions between mercury atoms. We use the Lennard-Jones potential to determine viscosity.[4] The viscosity is independent of the pressure of mercury.

B. Thermal conductivity

Each of the heavy particles transports the same kinetic energy as an electron because gas temperature equals electron temperature in the arc discharge. However, an electron moves much faster than any heavy particle and it also transports much more energy than any heavy particle in unit time. The number density of mercury atoms is, however, much larger than that of electrons. Therefore, we take mercury atoms and electrons into account to calculate thermal conductivity. We consider electron collisions with mercury atoms and ions; we use the momentum transfer collision cross section determined by England and Elford.[5] Hashiguchi and co-workers[1] give thermal conductivity of mercury gas as a function of temperature. The start of the electrons' contribution to thermal conductivity is dependent upon the gas pressure at high temperature because electron density is different for different gas pressures. We calculate electron density and ion density for the Hg/Na/Sc system taking all species into account.

C. Electrical conductivity

Electric charge is carried by electrons and ions. The mobility of electrons is much greater than that of ions and we take only electrons into account to determine the electrical conductivity of the working gas. Electron collisions with mercury atoms and with ions are taken into account. Hashiguchi and co-workers[1] give electrical conductivity of mercury gas as a function of temperature; it also depends on gas pressure even for lower temperatures. As described above, we calculate electron density and ion density taking all species into account to determine the electrical conductivity of the Hg/Na/Sc system.

D. Diffusion coefficients

Dakin and co-workers[2] calculated the diffusion coefficients of sodium atoms and sodium ions in mercury gas as a function of temperature, but collisions with ions were neglected. We calculate the diffusion coefficient of other particles in mercury gas using the fact that the diffusion coefficient is inversely proportional to the square root of the reduced mass of a moving particle with a target particle. The potential function is assumed to be the same as the one between a sodium atom and a mercury atom. The diffusion coefficient of scandium ions in mercury gas is calculated from the diffusion coefficient of sodium ions in the same way. We use them for the Hg/Na/Sc system.

IV. RADIATION POWER

A. Line radiation

We calculate radiation power taking 82 lines of mercury atoms, 64 lines of sodium atoms, 201 lines of scandium atoms and 92 lines of scandium ions into account. Two mercury lines (185.0 and 253.7 nm) and two sodium lines (589.0 and 589.6 nm) are resonance lines and are optically thick. We regard nine other strong mercury lines as optically thick

and all of the other lines as optically thin. Radiation power $U_{\text{thin},k}$ of an optically thin line k emitted from unit volume is expressed as

$$U_{\text{thin},k}=A_k\frac{g_k}{Z}n\exp(-E_k/k_BT),$$

where A_k is transition probability, g_k is statistical weight of excited level k, Z is partition function of species, n is number density of the species, E_k is energy of the excited level measured from the ground state of the species, and k_B is the Boltzmann constant. Data of the transition probabilities of these lines are provided by the following articles. The transition probabilities of mercury lines are collected from data obtained by Mosburg and Willke,[6] Stormberg and Schafer,[7] and Benck, Lawler, and Dakin.[8] We use the data of Wiese, Smith, and Miles,[9] for the transition probabilities of sodium lines and we use the data of Lawler and Dakin[10] and Fuhr and Wiese[11] for the transition probabilities of the atomic and ionic lines of scandium.

The calculation of radiation power emitted from optically thick lines is more complicated. We must take the effect of absorption in the gas into account. First, we calculate the radiation intensity of an optically thick line coming from an arbitrary direction into a point in the tube, taking absorption into account. Then, we determine its radial and axial components. By integrating over all directions, we obtain all radial and axial components of the radiation intensity of the line. Hence, we obtain the radiation intensity vector of the line at the point. The vector's divergence gives the radiation power of this line. The total radiation power from optically thick lines U_{thick} is obtained by summing all optically thick lines. Details of the method of calculation are described in Ref. 1.

B. Continuum radiation

We consider bremsstrahlung caused by electron-mercury atom collisions as continuum radiation power U_{ff}. An expression given by Zollweg, Lieberman, and Burnham[12] is used for the calculation of U_{ff}

$$U_{ff}(T)=\int B_\lambda(T)K_{e0}n_e n_{\text{Hg}}d\lambda,$$

$$K_{e0}=7.28\times10^{-30}\lambda^{2.19}\quad\text{for }\lambda>9.0\times10^{-5}\ \text{(cm)},$$

$$K_{e0}=3.30\times10^{-28}\lambda^{2.6}\quad\text{for }\lambda>9.0\times10^{-5}\ \text{(cm)},$$

where $B_\lambda(T)$ is radiation intensity of blackbody at wavelength λ, and the expression for K_{e0} is determined from data in Fig. 4 of Ref. 12. Integration with wavelength was made for several temperatures to obtain $U_{ff}(T)$. Zollweg and coworkers used Rockwood's data[13] for the momentum transfer cross section of an electron with a mercury atom. On the other hand, Hashiguchi and co-workers[1] used the cross section determined recently by England and Elford.[5] England and Elford gave a larger value for the cross section than Rockwood. We multiply $U_{ff}(T)$, which was determined on the basis of Rockwood's cross section, by a factor of 1.5 to obtain $U_{ff}(T)$ based on England and Elford's cross section. The results are expressed by the following analytical form:

$$U_{ff}(T)=2.24\times10^{-34}n_e n_{\text{Hg}}(8\times10^{-4}\ T-1.35)\times(\text{W/cm}^3)\quad\text{for }T>1688\ \text{K},$$

$$U_{ff}(T)=0\quad\text{for }T<1688\ \text{K}.$$

C. Method for the rapid calculation of optically thick radiation power

The method for calculating radiation power of optically thick lines U_{thick} described above is exact but it requires very long computing time. Moreover, it takes an intolerably long computing time to calculate an ac-driven discharge for several tens of periods. Thus, we need to devise a method for rapid calculation. The radiation power U_{thick} depends on temperature and the number densities of related species but it has a nonlocal character; it depends on whole profiles of temperature and densities in the tube. The radiation of the lamp is mainly emitted from the central part where physical quantities are almost axially uniform. Hence, to make a rapid calculation, we assume that U_{thick} depends on temperature and density profiles only in the radial direction.[14] The effect of convection on the energy equation is negligible in the axially uniform region because the amount of energy brought into this region by convection is taken out from this region by convection. Therefore, energy Eq. (4) is reduced to

$$\frac{\partial q}{\partial t}=\frac{1}{r}\frac{\partial}{\partial r}\left(rk\frac{\partial T}{\partial r}\right)+\frac{\partial}{\partial z}\left(k\frac{\partial T}{\partial z}\right)+\sigma E^2-U. \tag{14}$$

In the following, we consider a cylindrical volume which has enough height for an absorption calculation. First, we calculate temperature for an ac-driven discharge on the midplane of the volume solving Eq. (14) as a function of time; U_{thick} is calculated using the exact method described in Sec. IV A. We obtain various radial temperature profiles corresponding to various phases; the driving current is different for different phases.

The radial temperature profile is divided into two parts: the temperature at the center $T(0)$, and relative profile $F(r)$. Here, $F(r)$ is defined by

$$F(r)=\frac{T(r)-T(R)}{T(0)-T(R)}, \tag{15}$$

where $T(R)$ is the temperature at the sidewall. Profiles of $F(r)$ are different for different phases. We choose a number of typical profiles from them and we name the chosen profiles $F^s(r)$s.

The standard values of optically thick radiation power $U^s_{\text{thick}}(r)$ are determined in the following way:

(1) Select a profile $F^s(r)$ from the group of $F^s(r)$s.
(2) Determine $T^s(r)$ from $F^s(r)$ and appropriate value of $T^s(0)$.
(3) Calculate $U^s_{\text{thick}}(r)$ from $T^s(r)$ using the exact method together with number densities which are determined as a function of temperature.
(4) Prepare a spline formula to determine $U^s_{\text{thick}}(r)$ between two discrete values of $T^s(0)$.

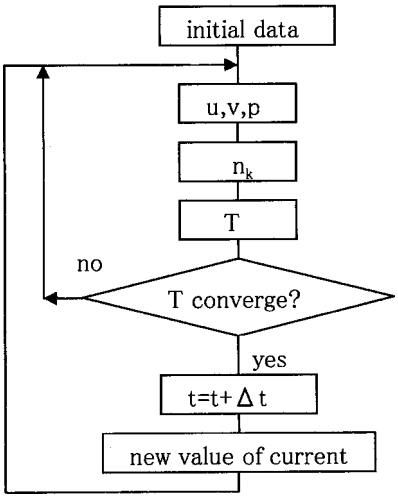

FIG. 2. Flow chart of numerical calculations as a function of time. Time t is advanced by Δt after temperature T converges.

In this way, we obtain $U^s_{\text{thick}}(r)s$ for discrete sets of $F^s(r)$s and an arbitrary value of $T(0)$. When $T(r)$ is given, optically thick radiation power is taken from data of $U^s_{\text{thick}}(r)$; $F^s(r)$ is selected so as to best fit $F(r)$, and then $U^s_{\text{thick}}(r)$ is obtained from $F^s(r)$ and $T(0)$.

A test calculation of temperature was made by solving Eq. (14) using the approximate method.[14] It should be noted that $U^s_{\text{thick}}(r)$ was determined from $T^s(r)$ but k and σ were determined from $T(r)$; $T^s(r)$ was not exactly the same as $T(r)$ because we used $F^s(r)$ instead of $F(r)$. We revised the value of temperature as an appropriate average of $T(r)$ and $T^s(r)$ to determine physical quantities at the next time step. Temperatures calculated using the exact method and the approximate method agreed within 2%.[14]

We used a workstation whose CPU was Alpha R21164 (667 MHz). It took 4.2×10^4 s to calculate over 20 half periods with the exact method and it took 176 s with the approximate method. The computing time was reduced by a factor of 240. We used the approximate method thereafter to save computing time.

V. NUMERICAL METHOD

Numerical procedure consists of three parts: calculation of velocities and pressure, calculation of number densities, and calculation of temperature. Figure 2 shows a flow chart of the numerical procedure: we determine u, v and p using previous values of temperature, we determine number densities using velocities and temperature, and we determine temperature using velocities and number densities. The procedure is repeated until temperature converges. Then, we increase time by Δt and the calculation is repeated. Each procedure is described in the following.

A. Velocities and pressure

Equations (1) through (3) are replaced by linearized finite difference equations; we linearize nonlinear terms replacing unknown variables with previously obtained values except one diagonal unknown. We use Patankar's semiimplicit method for pressure-linked equations[15] (SIMPLE for short); the continuity equation is used to determine pressure. Under-relaxation factors are used to stabilize numerical calculations.

B. Number densities

We determine particle fluxes using previously obtained temperature and number densities. Then, finite difference equations of Eqs. (8) through (10) reduce to the sum of several unknown number densities as a function of the known value. Hence, we obtain nonlinear algebraic equations including nine unknown number densities at each lattice point in the tube. We solve these equations using the Newton-Raphson method to obtain number densities.

C. Temperature

Internal energy and enthalpy consist of thermal energy and potential energy of ionization and dissociation. The ionization degree of mercury atoms is of the order of 10^{-3} and the amount of additives is less than 10^{-2} of the amount of mercury. The thermal energy of mercury atoms is dominant and other energies are negligible. Therefore, internal energy q and enthalpy h are reduced to

$$q=\frac{3}{2}n_{\text{Hg}}k_BT \quad \text{and} \quad h=\frac{5}{2}n_{\text{Hg}}k_BT. \tag{16}$$

Equation (4) is replaced by a linear implicit finite difference equation of temperature. To make linearization, we determine thermal conductivity, electrical conductivity, and radia-

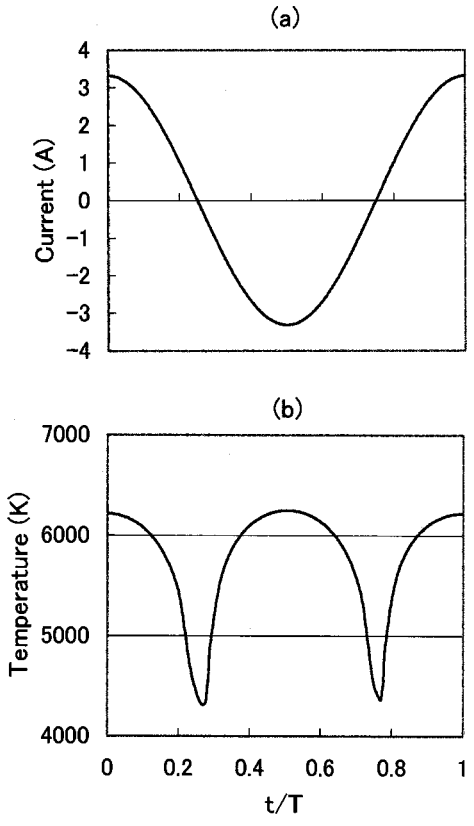

FIG. 3. Current (a) and temperature (b) at the center in the tube as a function of time t. Here, T means the period of driving alternating current.

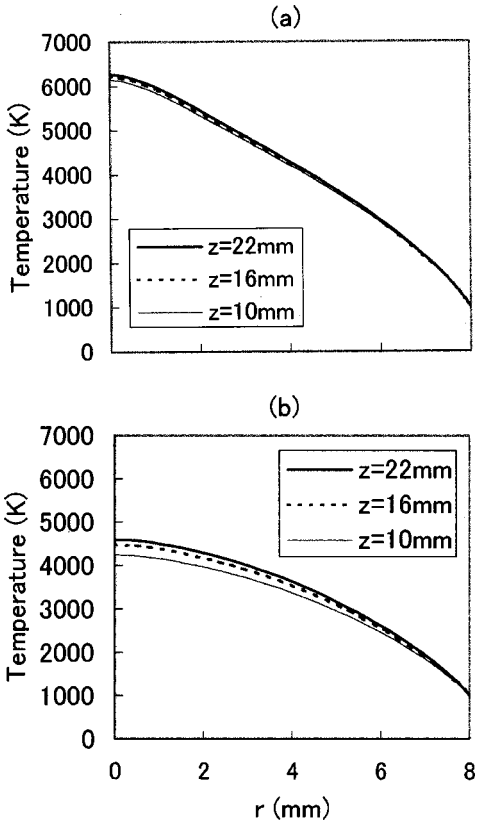

FIG. 4. Temperatures at three axial positions as a function of radial distance at the maximum current (a) and at the zero current (b). Here, three kinds of lines, i.e., thin solid, dotted and thick solid lines, show the radial density profiles at the axial positions of z=10 mm, 16 mm (center) and 22 mm, respectively. It is noted here that the three kinds of lines have the same meaning in the following figures.

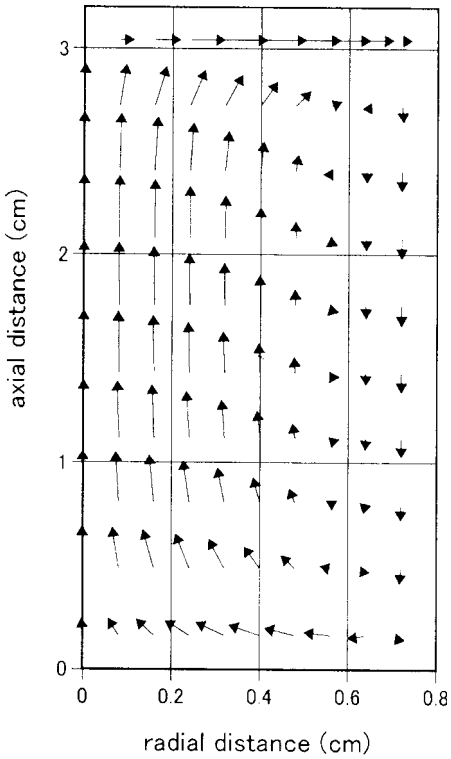

FIG. 5. Convection velocities in the tube at the maximum current. The maximum value of the axial velocity is 30 cm/s on the central axis.

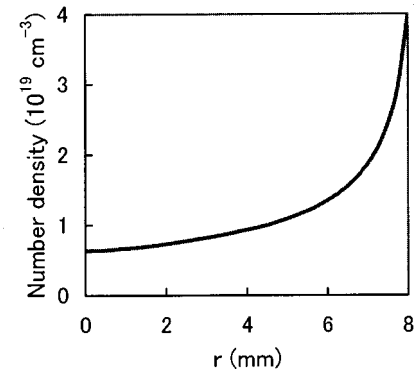

FIG. 6. Number density of mercury atoms at three axial positions as a function of radial distance r at the maximum current. The number density is almost independent of the axial position.

tion power using previous values of temperature and number densities. Axial electric field E is determined from electrical conductivity and the driving current; E is assumed to be uniform over the cross section of the tube. We use the under-relaxation method to obtain temperature.

VI. RESULTS AND DISCUSSION

Calculation was carried out for a 250 W lamp made by Japan Storage Battery Co., Ltd. The geometry of the lamp is schematically shown in Fig. 1; the inner diameter of the tube is 16 mm and the gap between electrodes is 32 mm. We put 31 lattice points along the radial direction from the center to the sidewall and we put 21 lattice points along the axial direction from electrode to electrode. The time step Δt is the period of driving current divided by 3200. Condensates of sodium iodine and scandium iodine as well as an amount of 34 mg of liquid mercury were introduced into the tube. Mass ratio of NaI to ScI_3 was 6.5:1. The coldest temperature T_c in the tube was unknown at operation. When $T_c=900$ K vapor pressures of NaI and ScI_3 are estimated to be 26.9 and 14.1 Pa,[16] respectively. When $T_c=950$ K they are 80 and 38.5 Pa. We made calculations for both values of T_c.

Convection velocities u and v are zero on the boundary. We specify temperature on the boundary. The temperature is assumed to be 1000 K on the sidewall and it is assumed to be 3000 K on the electrodes which are at the center on the upper

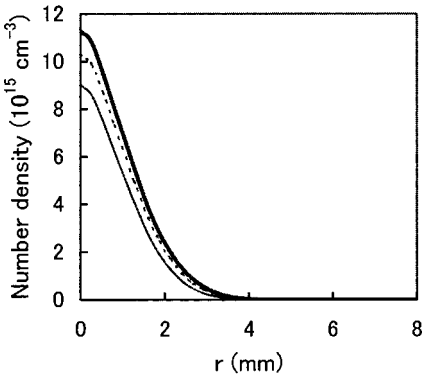

FIG. 7. Number density of mercury ions at three axial positions as a function of radial distance at the maximum current.

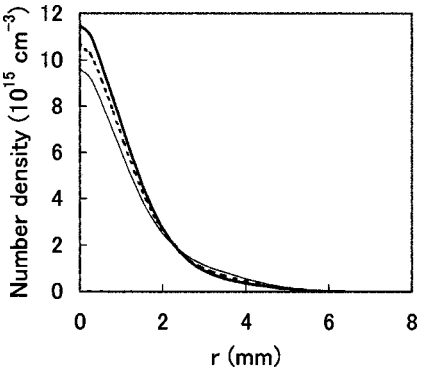

FIG. 8. Number density of electrons at three axial positions as a function of radial distance at the maximum current.

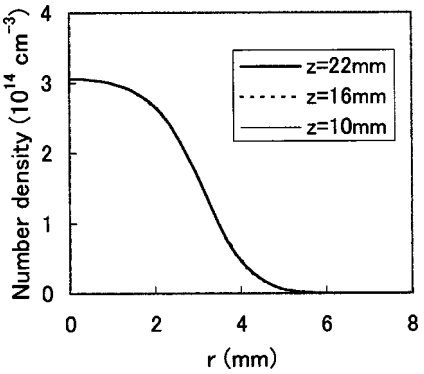

FIG. 10. Number density of scandium ions at three axial positions as a function of radial distance at the maximum current. Diffusion and axial drift are neglected.

and the lower boundaries. Temperature gradually decreases to 1000 K with increasing radial distance from the center. The lamp was driven by an ac current of 60 Hz; effective current was 2.34 A. Calculation was continued for 50 periods and results in the last period are shown in the following figures.

Figure 3 shows temperature at the center on the midplane as a function of time for $T_c = 950$ K; discharge current is also shown. The temperature at the center varies from 4500 to 6400 K in a cycle. The pressure varied from 0.49 to 0.56 MPa in a cycle. Figure 4 shows radial temperature profiles for three axial positions: z=10, 16, and 22 mm at the maximum current 4(a) and at zero current 4(b). The temperature profile is axially almost uniform at the maximum current but it increases slightly with increasing axial distance from the bottom of the tube. Figure 5 shows convection velocity at the maximum current; the gas ascends in the hot region and it descends near the wall. The axial velocity has a maximum value of 30 cm/s on the central axis.

Figures 6–16 show the number densities of various kinds of particles at the maximum current as a function of r for three axial positions shown in Fig. 4. Figure 6 shows the number density of mercury atoms. The pressure of mercury atoms is uniform in the tube and we obtain a smaller number density at higher temperature; the radial temperature profile at the maximum current is given in Fig. 4(a). The number density is almost independent of the axial position. Figures 7 and 8 show the number density of mercury ions and electrons, respectively. The number density has a maximum at the center where temperature is at maximum; mercury ions increase because of a sharp increase in the ionization degree with increasing temperature in spite of a decrease in the number density of mercury atoms shown in Fig. 6. The negative charge of electrons is mainly canceled by mercury ions. The difference between them shows the contribution of sodium and scandium ions. The number density of mercury ions and electrons has a tendency to increase slightly with increasing axial distance from the bottom. The cause of change in the number density of mercury atoms and electrons is explained by a change in temperature because the temperature profile given in Fig. 4(a) shows the same tendency; change in number density is amplified compared with change in temperature.

Figure 9 shows the number density of scandium ions. One of the remarkable differences in the profile compared with that for mercury ions (Fig. 7) is that it has a minimum at the center. Figure 10 shows the number density of scandium ions which was calculated without diffusion and axial drift. It should be noted here that our experimental data, which will be given in a following article, agree more closely with the results in Fig. 9. It is clear that the minimum at the center in Fig. 9 is caused by radial diffusion. The radial electric field was mainly determined by charges of mercury ions and electrons. It is directed outward near the center even though the number density of scandium ions has a minimum at the cen-

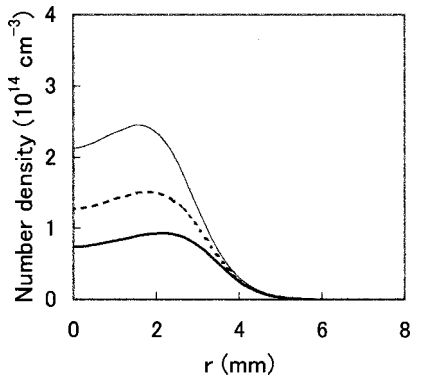

FIG. 9. Number density of scandium ions at three axial positions as a function of radial distance at the maximum current.

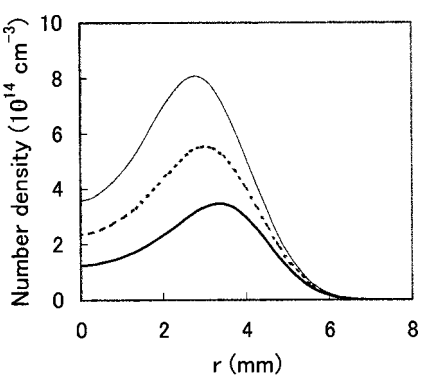

FIG. 11. Number density of sodium ions at three axial positions as a function of radial distance at the maximum current.

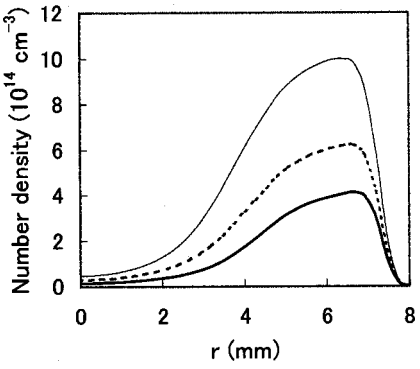

FIG. 12. Number density of sodium atoms at three axial positions as a function of radial distance at the maximum current.

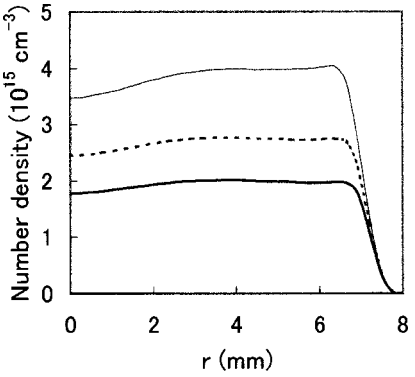

FIG. 14. Number density of iodine atoms at three axial positions as a function of radial distance at the maximum current.

ter. Figure 11 shows the number density of sodium ions. It shows a similar density profile to that of scandium ions though the minimum at the center is partly caused by a decrease in sodium atoms due to rarefaction by high temperature as is shown in Fig. 6; the ionization degree of sodium atoms is high enough near the center and a sharp increase in ion density like that shown in Fig. 7 did not occur in this case.

Figures 12–16 give the number densities of Na, Sc, I, NaI, and ScI_3. They show the same tendency as Figs. 9 and 11 in that the number density decreases with increasing axial distance from the bottom. All these particles resulted from metal-halide condensate which existed on the bottom of the tube. Vaporized particles were transported upward by an ascending convection flow in the hot region but some of them were lost by radial diffusion. Therefore, the supplied amount decreased with increasing axial distance from the bottom. Figure 10 shows that number density is axially uniform if diffusion and axial drift are negligible.

The radial density profile in Figs. 12– 16 is explained by the temperature effect shown in Fig. 6 together with dissociation and ionization which change as a function of temperature. The number density of sodium atoms (Fig. 12) shows a large dip at the center because the ionization degree is high there. The dip in the number density of scandium atoms at the center is smaller than that of sodium atoms because the ionization energy of scandium atoms is greater than that of sodium atoms. The number density of iodine atoms (Fig. 14) is uniform along the radial direction compared with that of sodium and scandium atoms. We neglected ionization of iodine atoms because the ionization degree is less than 1%. Figures 12–14 show that the number density of atoms decreases near the wall; the number of iodide molecules increases with decreasing temperature as is shown in Figs. 15 and 16.

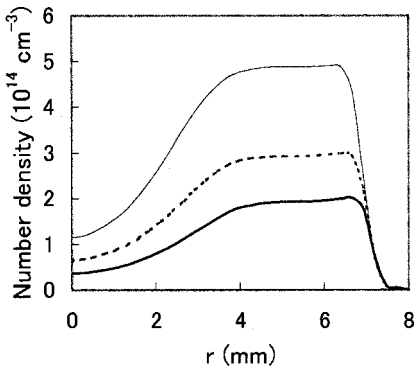

FIG. 13. Number density of scandium atoms at three axial positions as a function of radial distance at the maximum current.

It should be noted that the number densities presented in Figs. 6–16 are snapshots at the ascending current maximum where the axial electric field is directed upward. Figure 17 shows the number density of scandium ions at the descending current maximum where the axial electric field is directed downward. The number density at the descending current phase is smaller than that at the ascending current phase as is shown in Fig. 9 in the middle region of the discharge tube. Figures 18 and 19 show contour plots of the temperature and the number density of scandium ions in the discharge tube at the ascending current maximum and at the descending current maximum, respectively. More scandium ions exist near the lower boundary region ($z<8$ mm) at the descending current phase than that at the ascending current phase in contrast to the results shown in Figs. 9 and 17 for the middle region ($z = 10–22$ mm). This may be explained by the action of the axial electric field which pushes positive ions downward in the descending-current phase.

VII. CONCLUDING REMARKS

We use simple geometry as shown in Fig. 1 to neglect complex phenomena occurring near electrodes and therefore our model is unable to determine quantities related to electrodes such as a potential drop at the electrode. This is a problem which will be left for future work.

Optically thick lines are limited to resonance lines of mercury atoms and sodium atoms, and several strong lines of mercury atoms. However, several strong lines of scandium atoms seem to be optically thick under the operating condition studied here. We might define several strong lines of scandium atoms as optically thick if data of spectral width were available.

The approximate method to calculate U_{thick} was determined from the property of optically thick lines at the inner region of the discharge tube; the effect of absorption may decrease near the upper and lower boundaries and U_{thick}

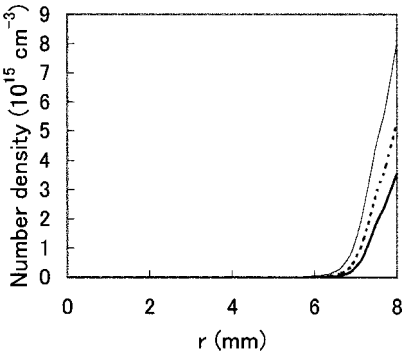

FIG. 15. Number density of sodium iodine molecules at three axial positions as a function of radial distance at the maximum current.

would then be larger than that obtained by the present calculation. To take the effect of the boundary into account, we simply double the value of U_{thick} at the lattice points nearest to the upper and lower boundaries. However, it is clear that a more precise method is desirable.

APPENDIX: PARTICLE FLUX DUE TO DIFFUSION IN MERCURY GAS

When we use the coordinate system which moves with convection velocity, we observe diffusion of various species in mercury gas; mercury gas itself is at rest in this coordinate. The general expression for diffusion flux[17] reduced for neutral species to

$$\boldsymbol{\phi}_{\text{n}}^{0} = -n_{,\text{Hg}} D_n \boldsymbol{\nabla}\left(\frac{n_{\text{n}}}{n_{\text{Hg}}}\right),$$

where ϕ_n^0 is particle flux of neutral species observed in this coordinate. As the pressure of mercury gas is uniform, n_{Hg} is expressed by

$$n_{\text{Hg}} = \frac{T^0 n_{\text{Hg}}^0}{T},$$

where superscript 0 means the standard value. Using this relation, we obtain

$$\phi_n^0 = -D_n\left(\boldsymbol{\nabla} n_n + \frac{n_n}{T}\boldsymbol{\nabla} T\right).$$

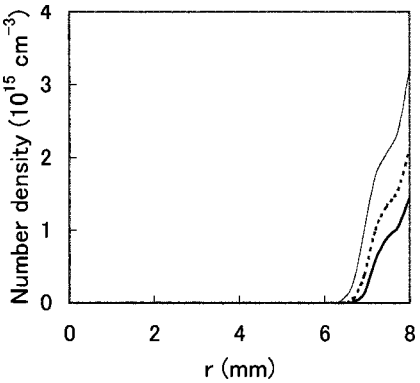

FIG. 16. Number density of scandium iodine molecules at three axial positions as a function of radial distance at the maximum current.

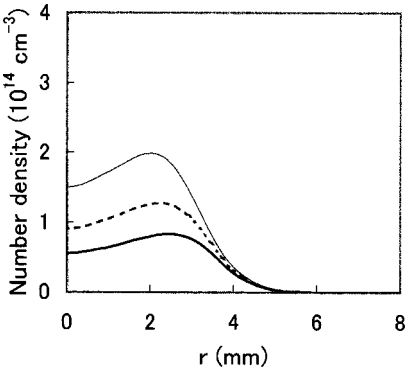

FIG. 17. Number density of scandium ions at three axial positions as a function of radial distance at the maximum current, but the current flows downward in comparison with Fig. 9 where the current flows upward.

Returning to the laboratory coordinate system, we obtain Eq. (11).

Particle flux of charged species is the same for the axial component except for the addition of the drift term. We now consider radial flux of charged species which includes ambipolar diffusion created by multiple kinds of ions. We first assume that temperature is uniform. The radial particle flux of each charge species in the moving coordinate with convection velocity is given by

$$\psi_{\text{Hg}^+}^0 = \mu_{\text{Hg}^+} n_{\text{Hg}^+} E_r - D_{\text{Hg}^+}\frac{\partial n_{\text{Hg}^+}}{\partial r},$$

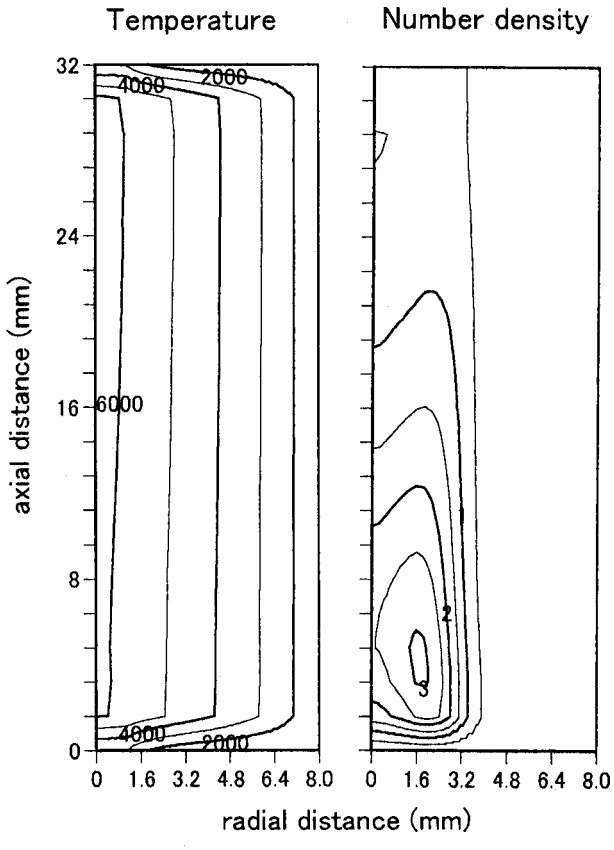

FIG. 18. Contour plots of temperature and number density of scandium ions in units of 10^{14} cm^{-3} at the ascending current maximum.

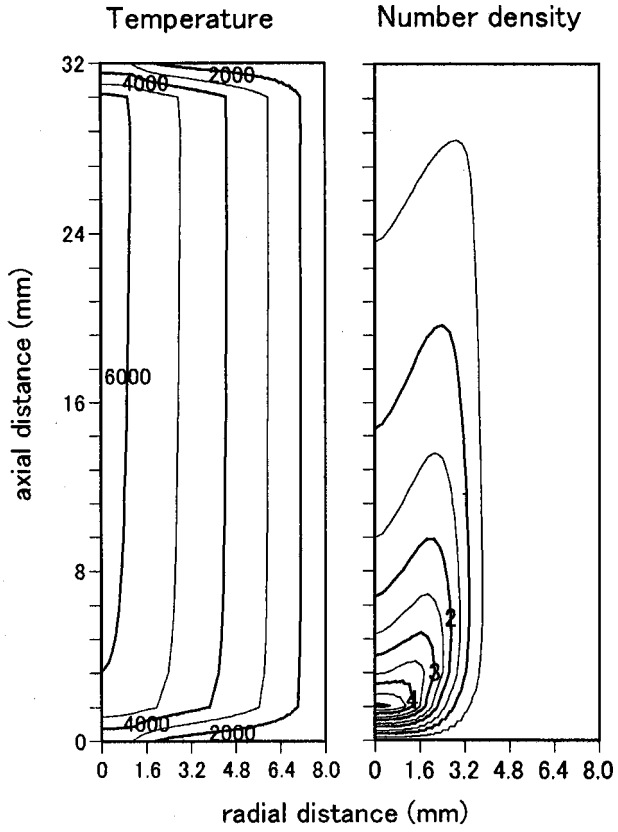

FIG. 19. Contour plots of temperature and number density of scandium ions in unit of 10^{14} cm^{-3} at the descending current maximum.

$$\psi^0_{\mathrm{Na}^+}=\mu_{\mathrm{Na}^+}n_{\mathrm{Na}^+}E_r-D_{\mathrm{Na}^+}\frac{\partial n_{\mathrm{Na}^+}}{\partial r},$$

$$\psi^0_{\mathrm{Sc}^+}=\mu_{\mathrm{Sc}^+}n_{\mathrm{Sc}^+}E_r-D_{\mathrm{Sc}^+}\frac{\partial n_{\mathrm{Sc}^+}}{\partial r}$$

and

$$\psi^0_{\mathrm{e}}=\mu_{\mathrm{e}}n_{\mathrm{e}}E_r-D_{\mathrm{e}}\frac{\partial n_{\mathrm{e}}}{\partial r},$$

where E_r is radial electric field, and electron mobility μ_{e} is negative. As the total ion flux equals electron flux, E_r is given by

$$E_r=\frac{D_{\mathrm{e}}\frac{\partial n_{\mathrm{e}}}{\partial r}-D_{\mathrm{Hg}^+}\frac{\partial n_{\mathrm{Hg}^+}}{\partial r}-D_{\mathrm{Hg}^+}\frac{\partial n_{\mathrm{Hg}^+}}{\partial r}-D_{\mathrm{Hg}^+}\frac{\partial n_{\mathrm{Hg}^+}}{\partial r}}{\mu_{\mathrm{e}}n_{\mathrm{e}}-\mu_{\mathrm{Hg}^+}n_{\mathrm{Hg}^+}-\mu_{\mathrm{Na}^+}n_{\mathrm{Na}^+}-\mu_{\mathrm{Sc}^+}n_{\mathrm{Sc}^+}}$$

$$\approx\frac{D_{\mathrm{e}}}{\mu_{\mathrm{e}}n_{\mathrm{e}}}\frac{\partial n_{\mathrm{e}}}{\partial r},$$

where we use the charge neutrality condition and where electron transport coefficients are much larger than ion transport coefficients. Using Einstein's relation, we obtain

$$E_r=-\frac{D_{\mathrm{Hg}^+}}{\mu_{\mathrm{Hg}^+}n_e}\frac{\partial n_e}{\partial r}=-\frac{D_{\mathrm{Na}^+}}{\mu_{\mathrm{Na}^+}n_e}\frac{\partial n_e}{\partial r}=-\frac{D_{\mathrm{Sc}^+}}{\mu_{\mathrm{Sc}^+}n_{\mathrm{e}}}\frac{\partial n_e}{\partial r}.$$

Finally, for ion species we obtain

$$\psi^0_{\mathrm{ion}}=-D_{\mathrm{ion}}\left(\frac{\partial n_{\mathrm{ion}}}{\partial r}+\frac{n_{\mathrm{ion}}}{n_e}\frac{\partial n_{\mathrm{e}}}{\partial r}\right).$$

This equation reduces to the well-known expression for ambipolar diffusion when $n_{\mathrm{ion}}=n_e$. When temperature is nonuniform, ψ^0_{ion} is given by

$$\psi^0_{\mathrm{ion}}=-D_{\mathrm{ion}}n_{\mathrm{Hg}}\left[\frac{\partial}{\partial r}\left(\frac{n_{\mathrm{ion}}}{n_{\mathrm{Hg}}}\right)+\frac{n_{\mathrm{ion}}}{n_{\mathrm{e}}}\frac{\partial}{\partial r}\left(\frac{n_{\mathrm{e}}}{n_{\mathrm{Hg}}}\right)\right]$$

$$=-D_{\mathrm{ion}}\left(\frac{\partial n_{\mathrm{ion}}}{\partial r}+\frac{n_{\mathrm{ion}}}{n_{\mathrm{e}}}\frac{\partial n_{\mathrm{e}}}{\partial r}+\frac{2n_{\mathrm{ion}}}{T}\frac{\partial T}{\partial r}\right).$$

Returning to the laboratory coordinate system, we obtain Eq. (12).

[1] S. Hashiguchi, S. Mori, and K. Tachibana, Jpn. J. Appl. Phys., Part 1 **36**, 6533 (1997).
[2] J. T. Dakin, T. H. Rautenberg Jr., and E. M. Goldfield, J. Appl. Phys. **66**, 4074 (1989).
[3] T. Ishigami: Proceeding of the 9th International Symposium on Science and Technology of Light Sciences, 2001, Ithaca, NY.
[4] J. O. Hirschfelder, C. F. Curtis and R. B. Bird, *Molecular Theory of Gases and Liquids* (Wiley, New York, 1954), Chap. 8.
[5] J. P. England and M. T. Elford, Aust. J. Phys. **44**, 647 (1991).
[6] E. M. Mosburg Jr. and M. D. Willke, J. Quant. Spectrosc. Radiat. Transf. **19**, 69 (1978).
[7] H. P. Stormberg and R. Scahfer, J. Appl. Phys. **54**, 4338 (1983).
[8] E. C. Benck, J. E. Lawler, and J. T. Dakin, J. Opt. Soc. Am. **6**, 11 (1989).
[9] W. L. Wiese, M. W. Smith and B. M. Miles, *Atomic Transition Probabilities* (NSRDS-NBS, 1969), Vol. II, p. 22.
[10] J. E. Lawler and J. T. Dakin, J. Opt. Soc. Am. **6**, 1457 (1989).
[11] J. R. Fuhr and W. L. Wiese, NIST Atomic Transition Probability Tables in *CRC Handbook*, 77th ed. (CRC, Boca Raton, FL), Vol. 10, p. 128.
[12] R. J. Zollweg, R. W. Lieberman, and R. Burnham, J. Quant. Spectrosc. Radiat. Transf. **18**, 133 (1977).
[13] S. D. Rockwood, Phys. Rev. A **8**, 2348 (1973).
[14] S. Hashiguchi, K. Hatase, S. Mori, and K. Tachibana, Proceedings of the 25th Annual Conference on Phenomena in Ionized Gases, Nagoya, Japan, 2001, Vol. 2, p. 241.
[15] S. V. Patankar, *Numerical Heat Transfer and Fluid Flow* (Japanese translation) (Morikita Shuppan, Tokyo, 1985).
[16] T. Ishigami, J. Illum, Engng. Inst. Jpn. (in Japanese) **81**, 1010 (1997).
[17] J. O. Hirschfelder, C. F. Curtis, and R. B. Bird, *Molecular Theory of Gases and Liquids* (Wiley, New York, 1954), Chap. 7.